Shortwave radiative closure experiment and direct forcing of dust aerosol over northwestern China

J. M. Ge,[1] J. P. Huang,[1] J. Su,[1] J. R. Bi,[1] and Q. Fu[1,2]

Received 8 September 2011; revised 1 November 2011; accepted 6 November 2011; published 20 December 2011.

[1] Modeled and observed solar diffuse fluxes at the surface usually have unacceptably large discrepancies. It is necessary to address and resolve these discrepancies in order to accurately calculate a reliable aerosol direct radiative forcing (DRF). We present and compare two methods of deriving dust aerosol optical properties from the MFRSR (Multi-Filter Rotating Shadowband Radiometer) observations and the AERONET products. The single-scattering albedo (SSA) values from MFRSR are found to be 10% less than those from the AERONET. This difference is mainly due to the different imaginary part of refractive index retrieved by the MFRSR compared to AERONET. These two sets of dust aerosol optical properties are used in the SBDART model to simulate the shortwave fluxes that are compared with the surface observations to perform the radiative closure experiment. The diffuse simulations using the AERONET-derived aerosol SSA may have significant discrepancies compared with the observed diffuse irradiances. The DRFs at the top of atmosphere (TOA) simulated with the MFRSR-derived aerosol optical properties are positive while the DRFs with the AERONET are negative. The sign of the DRFs at the surface and in the atmosphere using the MFRSR is the same as those using the AERONET while the magnitudes from the MFRSR are much larger. It indicates that dust aerosols with higher absorption as derived from the MFRSR heat the aerosol layer but cool the surface much more than those based on the AERONET, which may have an important impact on the boundary layer processes. **Citation:** Ge, J. M., J. P. Huang, J. Su, J. R. Bi, and Q. Fu (2011), Shortwave radiative closure experiment and direct forcing of dust aerosol over northwestern China, *Geophys. Res. Lett.*, *38*, L24803, doi:10.1029/2011GL049571.

1. Introduction

[2] Aerosol direct radiative forcing (DRF), which impacts the Earth-atmosphere radiation budget, is one of the most important factors for modeling climate and climate change. Dust DRF and changes thereof have been a scientific interest for decades and numerous works have been published [e.g., *Lacis et al.*, 1992; *Hansen et al.*, 1997; *Kaufman et al.*, 2001; *Slingo et al.*, 2006; *Forster et al.*, 2007; *Kim and Ramanathan*, 2008]. The aerosol DRFs have been derived based on direct observations, remote sensing retrievals and radiative transfer model simulations, which are further used to assess the potential influence of aerosol on climate. The key parameters for determining aerosol DRF are the wavelength-dependent aerosol optical properties including aerosol optical depth (τ, AOD), single scattering albedo (ω, SSA) and asymmetry factor (g, ASY). In order to accurately calculate aerosol DRF, the fundamental step is to determine these aerosol optical properties. To that end, a number of aerosol optical property inversion methods based on ground and satellite-based remote sensing have been developed [*Kaufman et al.*, 1997; *Holben et al.* 1998; *Martonchik et al.*, 1998; *Dubovik and King*, 2000; *Ge et al.*, 2010]. However, all these aerosol optical properties derived from observations and retrievals need to be validated before aerosol DRF can be accurately and adequately calculated. One effective way to validate these parameters is to use them as input to radiative transfer codes, reproduce the broadband irradiance (direct normal, diffuse and total) and then compare those modeled fluxes with direct observations, i.e. so-called radiative closure experiment.

[3] Several efforts have been made to realize this radiative closure experiment. *Kato et al.* [1997] examined the simulated and observed broadband fluxes at the Southern Great Plain (SGP) site in Oklahoma under cloud-free days. They found that measurements of the direct normal irradiance and model calculations agreed reasonably well; however the diffuse field irradiance was overestimated by 30.3 W/m^2 by the model. *Halthore and Schwartz* [2000] considered the correction of zero offset due to the infrared cooling of the pyranometer and did detailed comparisons between simulations and observations. Their results also showed a non-negligible discrepancy for diffuse irradiance. In a more recent work by *Halthore et al.* [2004], the difference between simulated and measured diffuse irradiances was much less than 10 W/m^2, which was believed to be associated with the instrumental uncertainty, for three of the five selected cases, but discrepancies greater than 10 W/m^2 still appeared in the other two cases. *Michalsky et al.* [2006] and *Wang et al.* [2009] reported that the closure experiments for both direct normal and diffuse broadband shortwave fluxes can be improved by better quantification of the input parameters and by better measurements of the solar irradiances.

[4] Previous closure experiments clearly show that unacceptably large uncertainties still exist in the surface downward diffuse fluxes in cloud-free sky with aerosols. Asian dust aerosol is considered to be a major component of aerosol mass loading over Northwest China and an important factor in climate forcing [*Huang et al.*, 2007]. Would one observe the similar discrepancy or not in the region of Northwest China? How different are the aerosol optical properties retrieved from different methods and how do these differences affect the closer experiment? What is the

[1]Key Laboratory for Semi-Arid Climate Change of the Ministry of Education and College of Atmospheric Sciences, Lanzhou University, Lanzhou, China.
[2]Department of Atmospheric Sciences, University of Washington, Seattle, Washington, USA.

0094-8276/11/2011GL049571

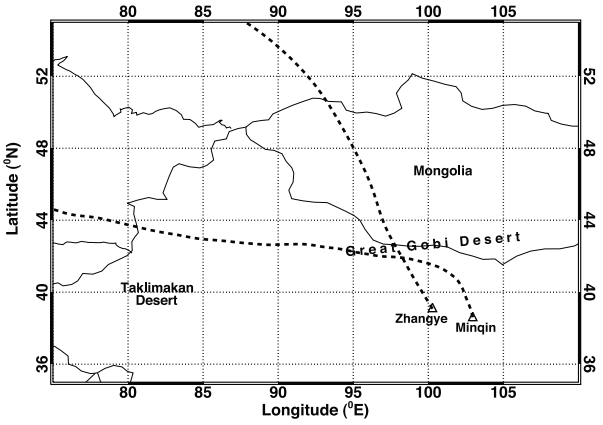

Figure 1. Geographic location of the two field experiment sites and HYSPLIT back trajectories analysis (dashed lines) at 3 km for the two cases.

difference of aerosol DRF if the closure experiments can or cannot be achieved? These questions motivated the efforts presented in this study.

[5] Two field experiments were conducted over Northwest China to examine the aerosol optical properties and radiative effects of Asian dust, respectively, by the U.S. Department of Energy Atmospheric Radiation Measurement (DOE/ARM) Program in 2008 and the Semi-Arid Climate and Environment Observation of Lanzhou University (SACOL) Program in 2010. These two experiments provide us an opportunity to answer above questions by examining Asian dust aerosol optical properties, comparing modeled and observed fluxes and determining aerosol DRF. In this paper, two cloud-free cases were selected from these two field campaigns. The modeling methods and observed data are described in section 2. Results of retrieved aerosol optical properties, closure experiments and calculated aerosol DRFs are shown in section 3. Major conclusions and discussions are given in section 4.

2. Measurement and Modeling Methods

[6] The measurements which we use in this paper are from two intensive field campaigns at sites located in Northwest China (Zhangye and Minqin, see the map in Figure 1). In 2008, the ARM Ancillary Facility (AAF) was established at Zhangye (39.082° N, 100.276° E, 1461m elevation), which is at the southern edge of the Gobi desert and in the semi-arid area of Northwest China, during the period of late April to mid June. The broadband total irradiance was measured with a Black and White Pyranometer (B&W, Eppley Laboratory, Newport, Rhode Island, USA) and the diffuse flux was obtained by a CM21 Pyranometer (Kipp & Zonen Inc., Delft, Netherlands). The direct normal irradiance was measured with two independent instruments which are a Normal Incidence Pyrheliometer (NIP, Eppley Laboratory) and CH1 (Kipp & Zonen Inc.), respectively. Column aerosol optical depth, single scattering albedo and asymmetry factor were derived from a CIMEL sun photometer and MFRSR. The case of April 24 (case1) was identified as a totally cloud-free day.

[7] The other field campaign site was set up in Badain Jaran Desert at Minqin (38.607°N, 102.959°E, 1373 m elevation), which is about 300km away to the southeast of Zhangye. In 2010, the SACOL Mobile Facility, including Precision Spectral Pyranometers (PSP, Eppley Laboratory), CHP1 (further improved accuracy and reliability on the legacy of CH1), NIP, CIMEL and MFRSR, was deployed at Minqin during May and June. The unshaded and shaded PSP were used to measure the total and diffuse irradiance, respectively. The direct normal irradiance was measured by both the NIP and CHP1 mounted on a Kipp & Zonen two-axis sun tracker. The case of May 22 (case2) was identified as a nearly clear-sky-day. The HYSPLIT (http://www.arl.noaa.gov/ready/hysplit4.html) model is used to analyze the back trajectories (dashed line in Figure 1) for the two cases.

[8] The Santa Barbara DISORT Atmospheric Radiative Transfer (SBDART, version 2.4) model with a 4-stream method is used for calculations of plane-parallel radiative transfer in our study [*Ricchiazzi et al.*, 1998]. The SBDART considers scattering and absorption processes that affect ultraviolet, visible and infrared radiation fields, which is flexible and could be readily adapted to our needs.

3. Results and Analysis

3.1. Model Input Parameters

[9] To calculate the shortwave fluxes at both the surface and top of the atmosphere (TOA) for the two selected cloud-free cases, the wavelength-dependent aerosol optical properties, integrated column water vapor, spectral surface albedo and ozone concentration are the required input parameters for the SBDART model. Data from two instruments, CIMEL and MFRSR, were used to determine aerosol optical properties. The CIMEL data were processed by AERONET [*Holben et al.*, 1998]. We used the MFRSR measurements to retrieve aerosol optical properties. The detailed retrieval method is presented by *Ge et al.* [2010, and references therein]. Note that 0.67μm is the common wavelength channel for CIMEL and MFRSR. Table 1 shows the values of τ, ω, g, Ångström exponent (α) and imaginary part of the refractive index (*i*k, REFI) from CIMEL and MFRSR, respectively at 0.67μm. The differences in τ, g and α between CIMEL and MFRSR are very small, on the order of 1%. However, for ω, the most important variable for aerosol DRF, the CIMEL and our MFRSR retrievals produced quite different results. The ω values from MFRSR are roughly 10% less than those from the CIMEL. Considering that the magnitude of ω is mainly dependent on the particle size distribution and refractive index (m = n + *i*k) [e.g., *Fu et al.*, 2009], we compare the volume-size distributions derived from the CIMEL and MFRSR in Figure 2 and the *i*k in Table 1. The dominance of the large particle mode (0.4 to 15μm) is a common feature (Figure 2) from the two retrievals in both cases. The MFRSR-derived particle volume concentrations and median radii of both the fine and

Table 1. Dust Aerosol Optical Properties Derived From CIMEL and MFRSR at 0.67μm for the Two Field Campaign Cases in Northwestern China

Case	Instrument	τ (0.67μm)	ω	g	α	*i*k
1	CIMEL	0.18	0.93	0.71	0.42	0.0035
	MFRSR	0.17	0.83	0.72	0.41	0.0100
2	CIMEL	0.16	0.94	0.72	0.49	0.0036
	MFRSR	0.15	0.86	0.71	0.49	0.0100

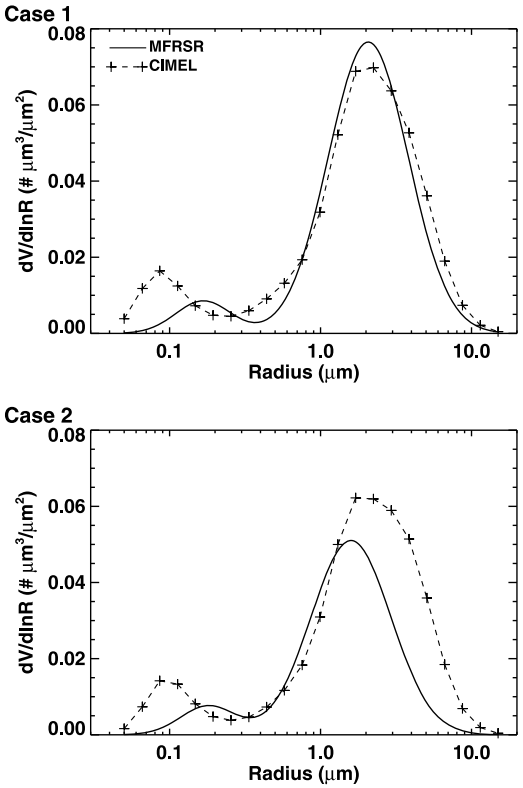

Figure 2. Volume-size distributions derived from MFRSR and CIMEL via inversion algorithms.

coarse modes are only slightly different from those retrieved by AERONET. To examine whether the different size distributions or the different refractive indices contribute to the differences in ω, we recalculated the Mie integrals using the MFRSR aerosol physical and optical properties but substituted the CIMEL-derived *i*k values. The bulk single-scattering albedos are 0.93 and 0.94 which are exactly the same as the CIMEL results for case 1 and 2, respectively. Thus, we can conclude that the difference in ω between our MFRSR retrievals and AERONET results are due to the different *i*k derived in the retrievals. The *i*k from the AERONET are 0.0035-0.0036 at 0.67μm, which are much smaller than 0.010 from our retrievals based on the MFRSR observations. Note that the *i*k value of dust aerosol given in the HITRAN database [*Rothman et al.*, 2009] is 0.08, which is also more than twice as large as *i*k from AERONET. Larger *i*k values from MFRSR lead to smaller SSAs, indicating that dust aerosol can absorb more solar energy than those estimated by the AERONET.

[10] For case1, the total column water vapor is taken from daily NCEP/NCAR reanalysis data. We obtain the broadband surface albedo (0.21) from CERES and assume that the surface type is composed of sand and vegetation; we then adjust the mixing fraction of sand and vegetation until the broadband surface albedo derived from the spectral distribution matches the CERES observation. For case2, the column water vapor is derived by integrating a standard desert water vapor profile adjusted for surface relative humidity and temperature observations. The broadband surface albedo (0.29) is also from CERES; however the spectral albedo is prescribed for the sand scene type in the SBDART model, which is then validated with the CERES observations. The ozone concentrations are taken from Total Ozone Mapping Satellite (TOMS) for both of the two cases.

3.2. Radiative Closure Experiment

[11] After obtaining the required model inputs (see section 3.1), we computed downward shortwave irradiances and made the comparisons with observations to perform radiative closure experiments. The observed shortwave broadband (0.3–3μm) total, diffuse, and direct normal irradiances over a wide range of solar zenith angles are compared with simulated fluxes for the two cases as illustrated in Figure 3.

[12] For case 1, the simulated direct normal irradiances obtained by using the aerosol optical properties from both the CIMEL and MFRSR agree well with the observations from sunrise to sunset. The daylight-averaged value of observed direct normal irradiance is 691.0 W/m^2. The fractional differences between simulations and observations are −0.4% and 0.6% for the CIMEL and MFRSR, respectively. For case 2, the simulated direct normal irradiances also agree well with observations. The fractional differences are within ±1% for both the CIMEL and MFRSR. These agreements between simulated and observed direct normal irradiances validate the dust aerosol optical depth retrievals from both CIMEL and MFRSR.

[13] For the diffuse irradiances, Figure 3 shows significantly larger discrepancies between the simulations and

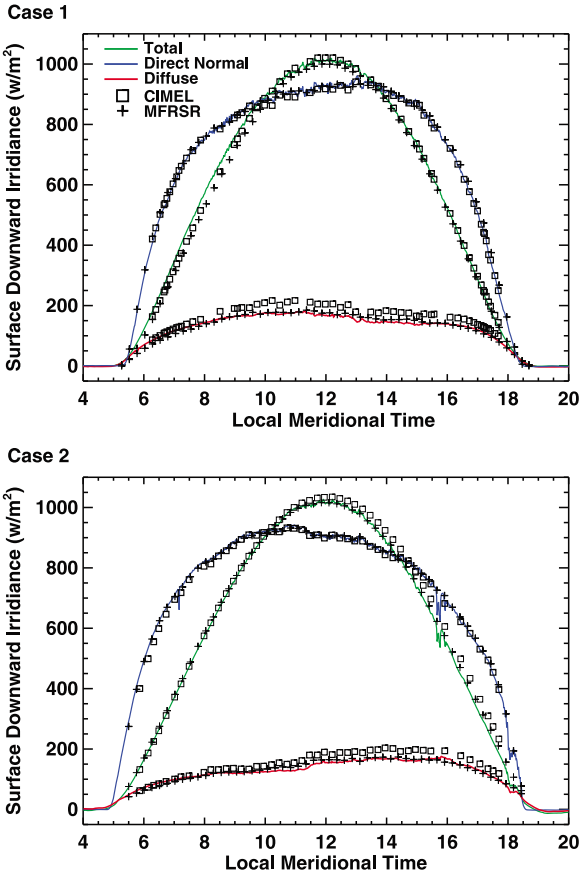

Figure 3. Surface irradiances calculated from MFRSR and CIMEL derived aerosol physical and optical properties compared to direct surface measurements at the two field campaign sites.

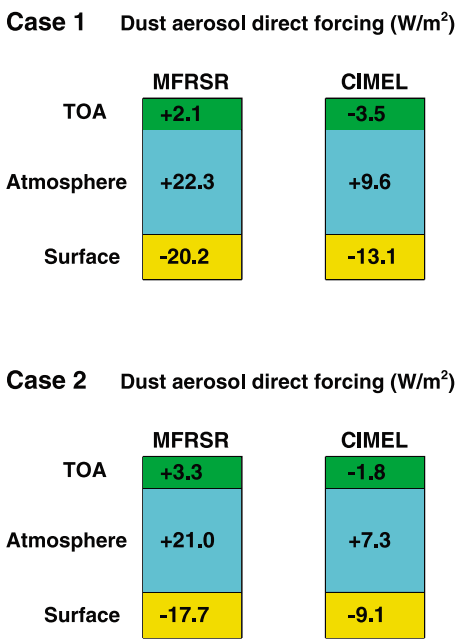

Figure 4. Summary of direct aerosol radiative forcing modeling results for both field study cases and measurements methods.

measurements by using the CIMEL aerosol optical properties than the MFRSR for both cases. For case 1, the daylight-averaged diffuse irradiance is 131.4W/m^2 and the fractional differences between modeled and observed daylight-averaged values are 18.1% and 0.7% for the CIMEL and MFRSR, respectively. The daylight-averaged diffuse irradiance of case 2 is 129.1W/m^2. The fractional differences between modeled and observed daylight-averaged values are 15.4% and 1.3% for the CIMEL and MFRSR, respectively. The RMS (root-mean-square) errors are 25.4 and 6.9 W/m^2 for the CIMEL and MFRSR, respectively in case 1, and 23.5 and 8.2 W/m^2 in case 2. For given aerosol optical depth, aerosols with smaller SSA absorb more, which leads to less downward diffuse irradiances. Our MFRSR-retrieved AOD and ASY at 0.67μm and the Ångström exponents are consistent with those from the AERONET products. However, by using larger SSA values of the AERONET, model produces larger diffuse field irradiance. The large differences between modeled and measured diffuse irradiances indicate that the AERONET product may overestimates the dust aerosol SSA.

[14] For the total irradiances, the daylight-averaged value is 607.0W/m^2 for the case 1. The simulations from MFRSR are slightly smaller than the observations while the modeling results from CIMEL are larger than the observations at noon. For the case 2, the daytime-averaged total irradiance is 645.6 W/m^2. The modeling results from MFRSR are close to the observations throughout the day while the simulations from CIMEL are larger during the afternoon.

3.3. Direct Radiative Forcing

[15] We have further computed downward shortwave irradiances under totally clear sky and have derived the dust aerosol direct radiative forcing by calculating the change in the net shortwave irradiances with and without the dust aerosols (SBDART) [*Ricchiazzi et al.*, 1998]. Figure 4 shows the dust aerosol DRF at the TOA, surface and in the atmosphere by considering different aerosol optical properties from the MFRSR and AERONET for both cases. For case 1, dust aerosol DRF at the TOA is 2.1 W/m^2 using the aerosol optical properties derived from the MFRSR. However, the DRF at the TOA using the AERONET derived aerosol optical properties has a negative value of −3.5 W/m^2. This is not surprising, because the aerosol can have a positive DRF at the TOA when the SSA is small, and a negative TOA DRF when the SSA is large for given surface albedo [*Ramanathan et al.*, 2001]. The surface DRFs derived by the MFRSR and AERONET are both negative, which are −20.2 and −13.1 W/m^2, respectively. The surface DRFs are much larger than the TOA DRFs, and thus large positive DRFs within the atmosphere occur as a consequence for both using the MFRSR and AERONET derived aerosol optical properties. The DRF results of case 2 are consistent with those of case 1. In case 2, The TOA DRF is +3.3 W/m^2 for the MFRSR and −1.8 W/m^2 for the AERONET. Dust aerosols reduce the solar fluxes reached at the surface and induce negative surface forcings of −17.7 and −9.1 W/m^2 for the MFRSR and AERONET, respectively. The MFRSR derived atmosphere DRF is 21 W/m^2 which is more than twice of that estimated by the AERONET.

[16] From the two cases, we can see that the sign of the TOA DRFs derived by the MFRSR and AERONET is opposite due to the different imaginary refractive indices and SSAs of the derived aerosol optical properties. The sign of the DRFs at the surface and in the atmosphere derived by the MFRSR is the same as those derived by the AERONET; however the magnitude of the surface and atmosphere DRFs from the MFRSR is much larger than that of the AERONET. It indicates that the main effect of dust aerosol is to heat the aerosol laden layer in the atmosphere but cool the surface, which may have impact on the boundary layer vertical mixing. Micro-pulse lidar measurements at the Zhangye and Minqin sites shown that the dust layer was largely confined between the surface and 4km; thus the majority of the atmospheric heating was in that layer.

4. Conclusion and Discussion

[17] The ARM ancillary Facility and SACOL Mobile Facility were deployed to Zhangye and Minqin in Northwestern China in 2008 and 2010, respectively. In this paper, we present and compare two methods of observing and deriving aerosol optical properties of dust by remote sensing for two cases. One is retrieved from MFRSR observations while the other is from the AERONET products. Our MFRSR-retrieved τ and g at 0.67μm and the Ångström exponents are consistent with those from the AERONET products. Both the MRSR- and AERONET-derived bimodal aerosol size distributions are dominated by large particles that have similar particle volume concentrations and median radii. However the ω values from MFRSR are 10% less than those from the AERONET. This difference is mainly due to the different ik values retrieved by the MFRSR compared to AERONET. The ik of the AERONET are 0.0035–0.0036 at 0.67μm. Our retrieved ik values are 0.01 which is more than twice as large as ik from AERONET.

[18] We used these two sets of dust aerosol optical properties as input to the SBDART model to simulate the shortwave flux reaching the surface and compare the simulations

with the direct surface observations to perform the radiative closure experiment. The simulated direct normal irradiances from both the CIMEL and MFRSR agree within ±1% overall with the observations for the two cases. However, the diffuse simulations using the AERONET derived aerosol ω have significant discrepancies compared with the observed diffuse irradiances.

[19] The differences of ω from the CIMEL and MFRSR can also cause quite different aerosol DRFs. The computation of the dust aerosol DRFs show that the TOA DRFs derived by the MFRSR are opposite in sign compared to the AERONET. However, the sign of the DRFs at the surface and in the atmosphere derived by the MFRSR is the same as that derived by the AERONET but the magnitude of the surface and atmosphere DRFs from the MFRSR are larger than that of AERONET values. It means that dust aerosol, in our MFRSR study, has higher absorption and stronger effects on heating the aerosol layer but cooling the surface than those estimated by the AERONET. The potential effects of dust aerosol on the thermodynamic structure and development of boundary layer are under investigation.

[20] **Acknowledgments.** This research is jointly supported by the National Basic Research Program of China (2012CB955302) and National Science Foundation of China under grant 41105108, 41175042 and 40725015 and the Fundamental Research Funds for the Central University (lzujbky-2011-2 and lzujbky-2011-4). QF is in part supported by the U.S. Department of Energy Grant No. DE-FG02-09ER64769. We thank Dr. Si-Chee Tsay and Qiang Ji of University of Maryland for providing high-quality data. We thank Prof. David S. Covert for useful comments and discussion.

[21] The Editor thanks two anonymous reviewers for their assistance in evaluating this paper.

References

Dubovik, O., and M. D. King (2000), A flexible inversion algorithm for retrieval of aerosol optical properties from Sun and sky radiance measurements, *J. Geophys. Res.*, *105*(D16), 20,673–20,696, doi:10.1029/2000JD900282.

Forster, P., et al. (2007), Changes in atmospheric constituents and in radiative forcing, in *Climate Change 2007: The Physical Science Basis. Contribution of Working Group I to the Fourth Assessment Report of the Intergovernmental Panel on Climate Change*, pp. 131–234, Cambridge Univ. Press, Cambridge, U. K.

Fu, Q., T. J. Thorsen, J. Su, J. M. Ge, and J. P. Huang (2009), Test of Mie-based single-scattering properties of non-spherical dust aerosols in radiative flux calculations, *J. Quant. Spectrosc. Radiat. Transfer*, *110*, 1640–1653, doi:10.1016/j.jqsrt.2009.03.010.

Ge, J. M., J. Su, T. P. Ackerman, Q. Fu, J. P. Huang, and J. S. Shi (2010), Dust aerosol optical properties retrieval and radiative forcing over northwestern China during the 2008 China-U.S. joint field experiment, *J. Geophys. Res.*, *115*, D00K12, doi:10.1029/2009JD013263.

Halthore, R. N., and S. E. Schwartz (2000), Comparison of model-estimated and measured diffuse downward irradiance at surface in cloud-free skies, *J. Geophys. Res.*, *105*(D15), 20,165–20,177, doi:10.1029/2000JD900224.

Halthore, R. N., M. A. Miller, J. A. Ogren, P. J. Sheridan, D. W. Slater, and T. Stoffel (2004), Further developments in closure experiments for diffuse irradiance under cloud-free skies at a continental site, *Geophys. Res. Lett.*, *31*, L07111, doi:10.1029/2003GL019102.

Hansen, J., M. Sato, and R. Ruedy (1997), Radiative forcing and climate response, *J. Geophys. Res.*, *102*, 6831–6864, doi:10.1029/96JD03436.

Holben, B. N., et al. (1998), AERONET: A federated instrument network and data archive for aerosol characterization, *Remote Sens. Environ.*, *66*, 1–16, doi:10.1016/S0034-4257(98)00031-5.

Huang, J., P. Minnis, Y. Yi, Q. Tang, X. Wang, Y. Hu, Z. Liu, K. Ayers, C. Trepte, and D. Winker (2007), Summer dust aerosols detected from CALIPSO over the Tibetan Plateau, *Geophys. Res. Lett.*, *34*, L18805, doi:10.1029/2007GL029938.

Kato, S., T. P. Ackerman, E. E. Clothiaux, J. H. Mather, G. G. Mace, M. L. Wesely, F. Murcray, and J. Michalsky (1997), Uncertainties in modeled and measured clear-sky surface shortwave irradiances, *J. Geophys. Res.*, *102*, 25,881–25,898, doi:10.1029/97JD01841.

Kaufman, Y., D. Tanré, L. Remer, E. Vermote, A. Chu, and B. Holben (1997), Operational remote sensing of tropospheric aerosol over land from EOS/MODIS, *J. Geophys. Res.*, *102*, 17,051–17,068.

Kaufman, Y. J., D. Tanre, O. Dubovik, A. Karnieli, and L. A. Remer (2001), Absorption of sunlight by dust as inferred from satellite and groundbased remote sensing, *Geophys. Res. Lett.*, *28*, 1479–1482, doi:10.1029/2000GL012647.

Kim, D., and V. Ramanathan (2008), Solar radiation budget and radiative forcing due to aerosols and clouds, *J. Geophys. Res.*, *113*, D02203, doi:10.1029/2007JD008434.

Lacis, A., J. Hansen, and M. Sato (1992), Climate forcing by stratospheric aerosols, *Geophys. Res. Lett.*, *19*, 1607–1610, doi:10.1029/92GL01620.

Martonchik, J. V., D. J. Diner, B. Pinty, M. M. Verstraete, R. B. Myneni, Y. Knyazikhin, and H. R. Gordon (1998), Determination of land and ocean reflective, radiative and biophysical properties using multi-angle imaging, *IEEE Trans. Geosci. Remote Sens.*, *36*, 1266–1281.

Michalsky, J. J., G. P. Anderson, J. Barnard, J. Delamere, C. Gueymard, S. Kato, P. Kiedron, A. McComiskey, and P. Ricchiazzi (2006), Shortwave radiative closure studies for clear skies during the Atmospheric Radiation Measurement 2003 Aerosol Intensive Observation Period, *J. Geophys. Res.*, *111*, D14S90, doi:10.1029/2005JD006341.

Ramanathan, V., P. J. Crutzen, J. L. Kiehl, and D. Rosenfeld (2001), aerosols, climate, and the hydrological cycle, *Science*, *294*, 2119–2124, doi:10.1126/science.1064034.

Ricchiazzi, P., S. Yang, C. Gautier, and D. Sowle (1998), SBDART: A research and teaching software tool for plane-parallel radiative transfer in the Earth's atmosphere, *Bull. Am. Meteorol. Soc.*, *79*(10), 2101–2114, doi:10.1175/1520-0477(1998)079<2101:SARATS>2.0.CO;2.

Rothman, L. S., et al. (2009), The HITRAN 2008 molecular spectroscopic database, *J. Quant. Spectrosc. Radiat. Transf.*, *110*, 533–572, doi:10.1016/j.jqsrt.2009.02.013.

Slingo, A., et al. (2006), Observations of the impact of a major Saharan dust storm on the atmospheric radiation balance, *Geophys. Res. Lett.*, *33*, L24817, doi:10.1029/2006GL027869.

Wang, P., W. H. Knap, P. Kuipers Munneke, and P. Stammes (2009), Clear-sky shortwave radiative closure for the Cabauw Baseline Surface Radiation Network site, Netherlands, *J. Geophys. Res.*, *114*, D14206, doi:10.1029/2009JD011978.

J. R. Bi, Q. Fu, J. M. Ge, J. P. Huang, and J. Su, Key Laboratory for Semi-Arid Climate Change of the Ministry of Education and College of Atmospheric Sciences, Lanzhou University, Lanzhou 730000, China. (gejm@lzu.edu.cn)